A new methodology for the analysis of two-dimensional fire spread simulations.

Francis M. Fujioka

USDA Forest Service, 4955 Canyon Crest Drive, Riverside, California 92507, USA.
Email: ffujioka@fs.fed.us

Abstract

Technologies now exist to simulate and observe fire spread at spatial resolutions on the order of 30 meters. The FARSITE modeling system recently introduced to the US fire management community provides two-dimensional fire spread simulations from a laptop computer, given topography, fuels, and weather information. The quality of the fire spread simulations is subject to examination. This paper describes a new methodology for the error analysis of two-dimensional fire spread simulations, from concurrent observations of actual fire spread. The methodology provides for construction of error bounds on model-based fire perimeter projections, which delimit the area within which the actual fire perimeter will be found at the predicted time, with specified probability. A case study demonstrates the capabilities and performance characteristics of FARSITE in the early stages of a wildfire that occurred in southern California, in summer 1996.

Introduction

Wildland fire models predict fire behavior, given the fuels, weather and topography. Some fire models have a long history, including the Rothermel spread model (Rothermel, 1972) in the USA, the Canadian model (Forestry Canada Fire Danger Group, 1992), and the McArthur model of Australia (McArthur, 1967; Noble et al., 1980). All of these models can err significantly in predicting the spread rate of fire. A system is needed to quantify the errors in fire spread models, particularly for two-dimensional fire spread models.

Finney (1998) recently introduced a personal computer-based fire modeling system in the USA that simulates fire spread in two dimensions, including surface fires and crown fires. The surface fire component incorporates the Rothermel model, with modifications by Albini (1976). Called FARSITE, the system utilizes the Rothermel model to determine the local maximum fire spread rate from a point as a function of the local fire environment variables. It then describes the local pattern of spread from the point by an ellipse. The process is repeated for as many points around the fire perimeter as specified by simulation parameters, and the envelope that contains all of the local ellipses constitutes the new fire perimeter. This method of propagating the fire front, known as Huygens' principle, was described by Richards (1995).

This paper describes research intended to develop a suite of modeling tools to plan and support fire operations. Weather models simulate the spatial and temporal variations of wind, temperature, and relative humidity that influence fuel moisture and fire spread. A fire spread model accounts for the combined effects of weather, fuel and terrain conditions. A statistical model analyzes the difference between simulated and observed fire spread to determine the magnitude and spatial/temporal variability of the fire spread simulation errors. The error analysis can be conducted on any appropriate combination of weather and fire spread models.

The following section explains the spread model error measure and a two-dimensional error function. A simple example of an error analysis is provided. I then introduce a random error component, and discuss its treatment. Finally, I analyze a fire simulation generated by FARSITE, for an actual fire that occurred in southern California, in summer 1996.

Definition of fire spread model error

Suppose we are given a fire perimeter P_0 at an initial time t_0, from which we model fire spread that results in the perimeter P_m at time t_1. Suppose further that the actual fire grows to the perimeter P_a in the same period of time. We can map and quantify the differences between the simulated and actual fires in two-dimensional space, by examining their respective areas in the sectors of P_m (Figure 1).

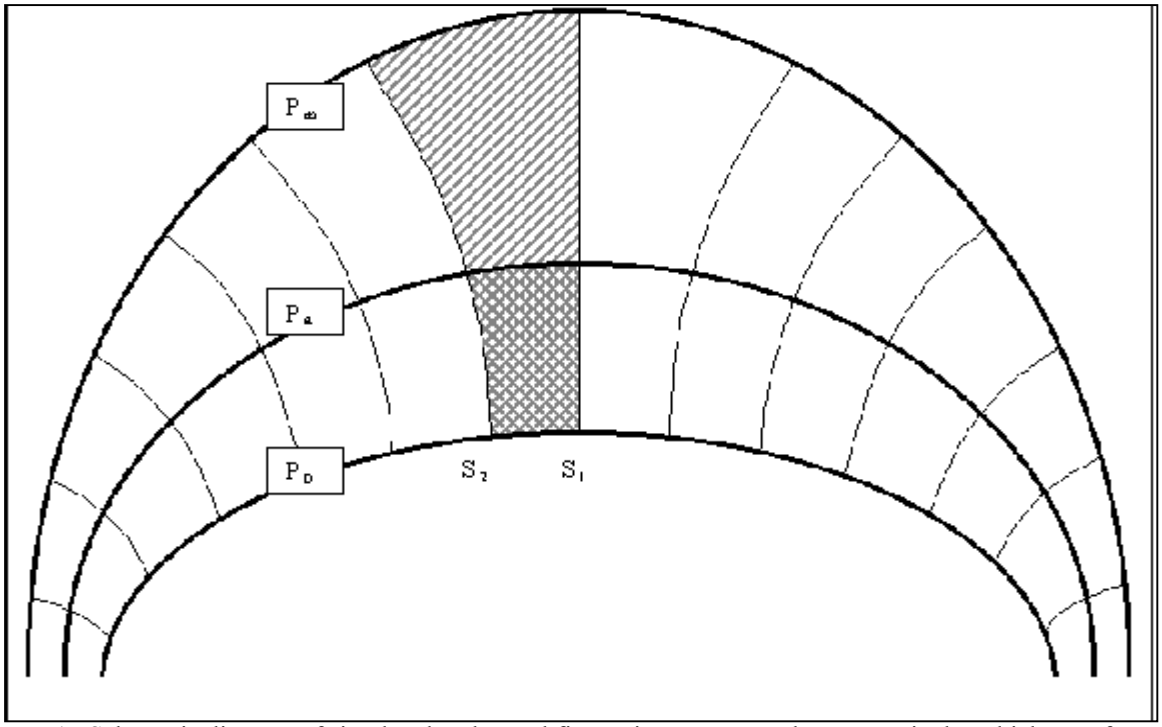

Figure 1. Schematic diagram of simulated and actual fire perimeters, P_m and P_a respectively, which start from an initial perimeter P_0. The cross-hatched area measures fire growth within the sector (s_1, s_2) for the actual fire, while the simulated fire also extends over the area marked by diagonals.

Let the sector boundaries s_i denote the orthogonal trajectories generated by the spread model. Within the sector (s_1,s_2), let A_a denote the area bounded by the initial and actual perimeters (cross-hatched area in Figure 1), and A_m the area similarly bounded by the initial and simulated fire perimeters (hatched areas, including A_a). Let $E(s_1,s_2,t_0,t_1)$ represent the ratio of the areas:

$$E(s_1,s_2,t_0,t_1)=\frac{A_a(s_1,s_2,t_0,t_1)}{A_m(s_1,s_2,t_0,t_1)} \tag{1}$$

We use E in (1) to be a measure of the error in P_m. It expresses the difference between the simulated and actual fires, at a spatial resolution of our choice, specified by the arguments of E. It also scales to the ratio of the mean burn paths of the actual and simulated fires within the sector. Generally, the factor governing spatial resolution will be the resolution of the actual fire perimeter data. E indicates a goodness of coverage of the simulated spread, in comparison to the actual spread within the sector, if the sector is chosen so that the actual perimeter is approximately orthogonal to the sector boundaries. Within the limits of the data, the sector can be chosen small enough to satisfy orthogonality to an arbitrary degree of accuracy. The mathematical details are given by Fujioka (2001).

We can use the error measure E around the perimeter of the fire to assess the two-dimensional variability of the fire spread model error. We calculate E within consecutive sectors around the entire perimeter, from which we build an error function, $B(s_j)$, where the subscript j indexes each sector. Let s_j be the midpoint of the sector.

$$B(s_j,t_1)=E(s_i,s_k,t_0,t_1), \quad s_j-s_i=s_k-s_j \tag{2}$$

B is a discrete function, but assume we can interpolate it to obtain a continuous measure of spread model error around the fire perimeter. B summarizes information about the spatial accuracy of the fire spread model. Ideally, $B(s,t_1)$ =1, in which case the spread model burns the same area that the actual fire does within each sector, and at least approximates the shape of the actual fire.

Moreover, if the model error is consistent over time, B can be used to correct the model predictions at succeeding time steps. Let $R_c(s,t_2)$ denote the spread rate thus corrected:

$$R_c(s,t_2)=R(s,t_2)B(s,t_1) \tag{3}$$

Generally, B varies in space *and* time.

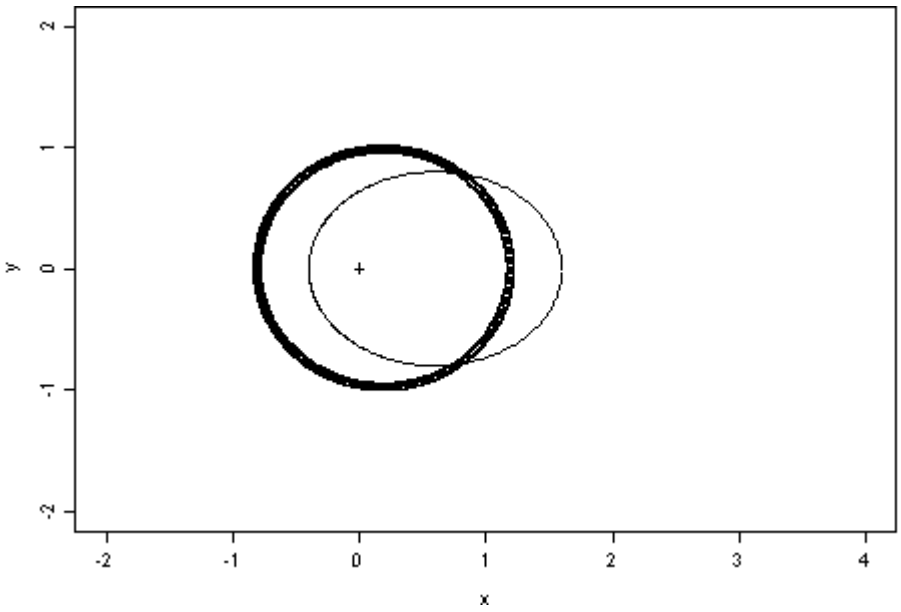

Figure 2. A hypothetical example in which a fire is predicted to burn elliptically with an eccentricity of 0.2 (heavy line), but actually burns as an ellipse with an eccentricity of 0.6 (thin line). The cross marks the origin of the fire.

Example of error analysis of an elliptic fire

Suppose that a fire grows elliptically west to east with eccentricity ε (Figure 2). Assume that the origin of the fire is the left focus of the ellipse, and set the origin of a two-dimensional polar coordinate system there. Let the length of the major axis be $2\alpha>0$; then the length of the radius vector is a function of θ:

$$r(\theta) = \frac{\alpha(1-\varepsilon^2)}{1-\varepsilon\cos\theta}, \quad 0 \le \theta < 2\pi, 0 \le \varepsilon < 1 \tag{4}$$

Note that α determines the size of the ellipse and ε dictates its shape. An eccentricity of zero produces a circular fire perimeter, a less likely case than a non-zero ε. In the latter case, the fire has a preferred spread direction, where θ equals zero. An alternative parameterization of elliptical shape is the length to breadth ratio, ρ, which is the ratio of the length of the major axis to the minor axis. Let 2β be the length of the minor axis. Then

$$\varepsilon^2 = \frac{\alpha^2 - \beta^2}{\alpha^2} \tag{5}$$

by definition, so

$$\rho = \left(\frac{1}{1-\varepsilon^2}\right)^{\frac{1}{2}} \tag{6}$$

Let *k* denote either the simulated or actual fire. Then the area of the sector in (θ_1, θ_2) is given by

$$\begin{aligned} A_k(\theta_1, \theta_2, 0, r_k) &= \int_{\theta_1}^{\theta_2} \int_0^{r_k} r dr d\theta \\ &= \frac{\alpha^2(1-\varepsilon_k^2)}{2}\left[\frac{\varepsilon_k \sin\theta}{1-\varepsilon_k\cos\theta} + \left[\frac{2}{\sqrt{1-\varepsilon_k^2}}\tan^{-1}\left(\sqrt{\frac{1+\varepsilon_k}{1-\varepsilon_k}}\tan\frac{\theta}{2}\right)\right]\right]_{\theta_1}^{\theta_2} \end{aligned} \tag{7}$$

The computation of *E* (equation 1) in sectors around the perimeter of the example yields the error function *B* (equation 2) shown in Figure 3. A perfect simulation would result in *B* equal to one everywhere. In our

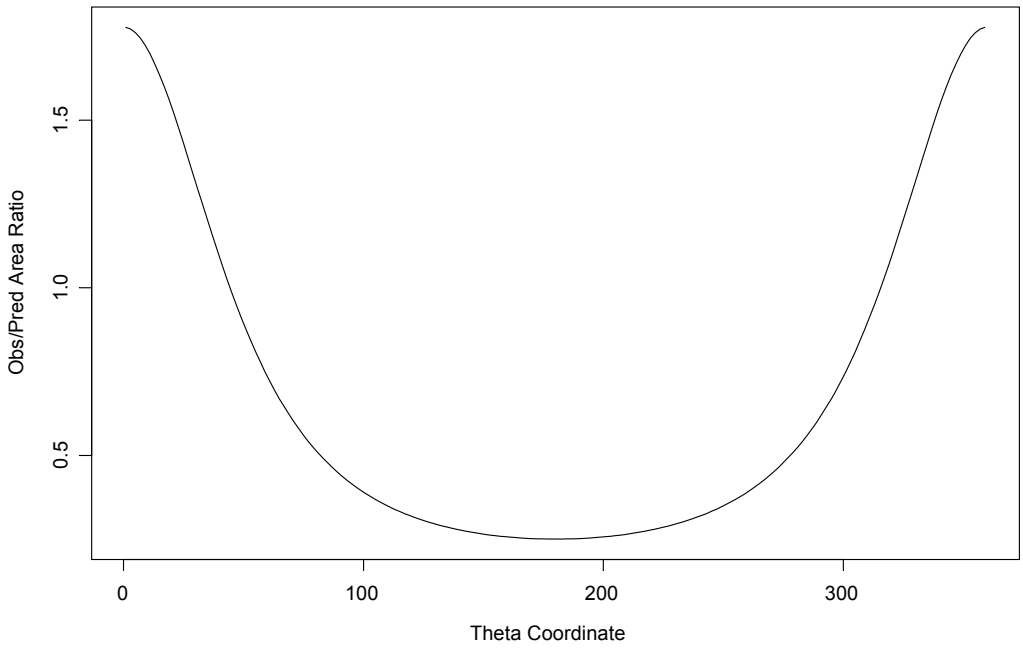

Figure 3. Error function *B* for the fire example in Figure 2.

example, *B* attains a maximum value of approximately 1.75 in the direction of the heading fire, and a minimum value of 0.25 in the direction of the backing fire. *B* is symmetric about 180°, because the simulated and actual perimeters are also symmetric about the x-axis. Note that *B* only approximates the continuous spatial variations of the error in the spread prediction, because the elements of *B* are located at discrete points around the fire perimeter, each representing a sector calculation.

Assuming that the spread model error characteristics will persist into the next time period, we can use *B* to correct for the error observed in the current period. The correction factor must retard the predicted spread when the model overestimated, and advance it when spread was underestimated. *E* is such a correction factor. However, the integrand function in the area calculation (7) is the square of *r*, because *r* is a scaling factor in the polar coordinate system. We want a correction factor of the form r_a/r_m (ratio of the mean radii of the actual and modeled fires, respectively) which we obtain from the square root of *E*, hence of *B*. Our corrected prediction at time t_2 is therefore

$$r_{t_2}(\theta) = r_a(\theta) + \frac{(\alpha_{t_2} - \alpha_{t_1})(1-\varepsilon_m^2)}{1-\varepsilon_m \cos\theta}\sqrt{B(\theta)} \tag{8}$$

where the subscript t_1 denotes the current time step.

The first term on the right describes the actual fire perimeter at time t_1 in our example; the second term is the incremental growth, corrected for the error observed in the current step. Thus, equation (8) incorporates information external to the spread model, namely the current position of the actual fire, $r_a(\theta)$, and the proportional spread of the actual fire, relative to the spread model, $\sqrt{B(\theta)}$. The positions of the simulated and actual fires at time t_2 are depicted in Figure 4, including corrected and uncorrected simulations.

The position corrected perimeter is the result of incorporating the actual perimeter location after the first time step, but not the correction factor. The fully corrected perimeter considerably improves upon both the uncorrected and the position corrected simulation at the second step, emphasizing the importance of the error function information, in this case. In fact, if we were to evaluate *B* for the uncorrected simulated and actual perimeters of the second time period in Figure 4, it would be the same result as for the first time period.

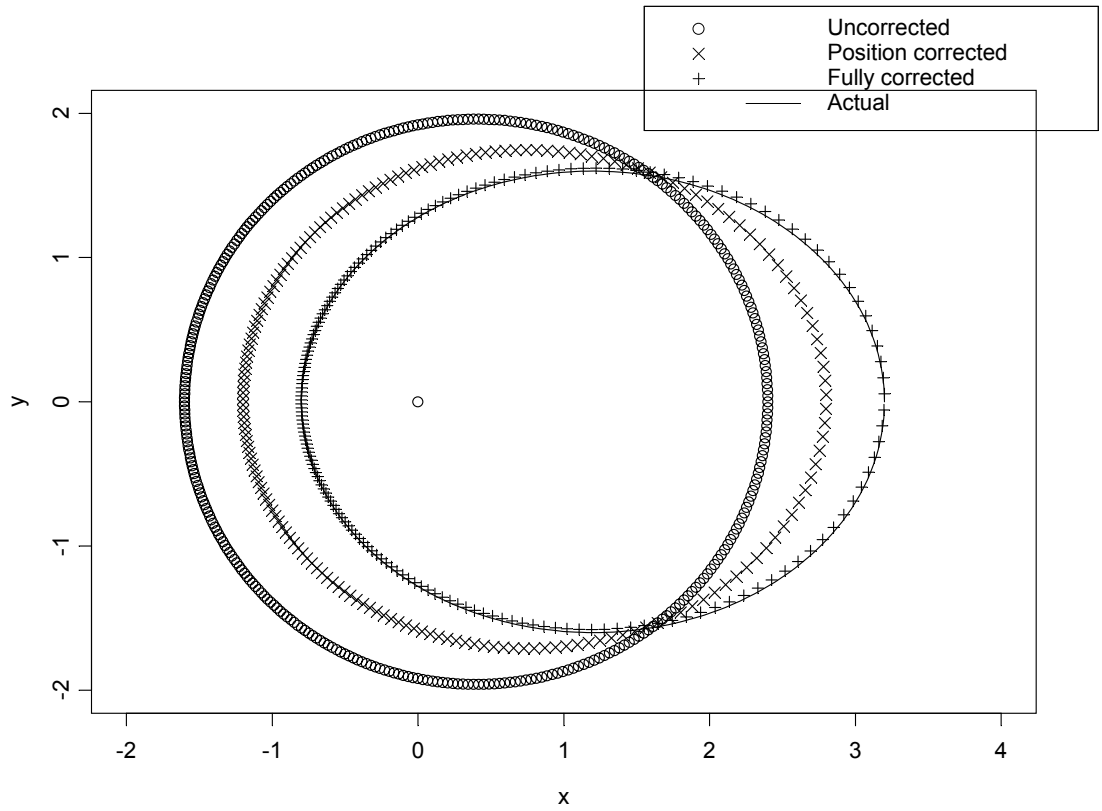

Figure 4. Fire perimeter plots at time t_2 of the example. The fully corrected perimeter occupies nearly the same position as the actual perimeter.

The eccentricity of the corrected perimeter has been considerably modified, due to the incorporation of the actual perimeter location at the end of the first time period, and to the influence of the correction factor $\sqrt{B(\theta)}$ in equation (8). The position corrected perimeter effectively ignores the correction factor by setting B to 1 for all θ. The example also demonstrates the importance of describing the variability of error around the perimeter, and not only in one direction.

Analysis of random spread model errors

We now consider the preceding example when E is a random variable. Suppose, for example, that E follows a lognormal distribution:

$$\ln \frac{A_a}{A_m} \sim N(\mu, \sigma^2) \tag{9}$$

Figure 5 shows an example of fire perimeter data with random points that fit the probability model in (9). Suppose we sampled the spread distances (radii) directly, and obtained the lognormal parameters given above. The spatial confidence interval for the true perimeter is derived from a lognormal distribution with variance s^2. Under the null hypothesis that the simulated fire covers the same area as the actual fire would *on average*, the spread model can be used to construct a spatial confidence interval for the simulated perimeter.

At any given time t, let R(θ) denote the true perimeter point along the radial in direction θ. Then an approximate 1-α confidence interval for ln R(θ) derives from

$$\frac{\ln R(\theta) - \ln r(\theta)}{s} \sim N(0,1) \tag{10}$$

from which we obtain

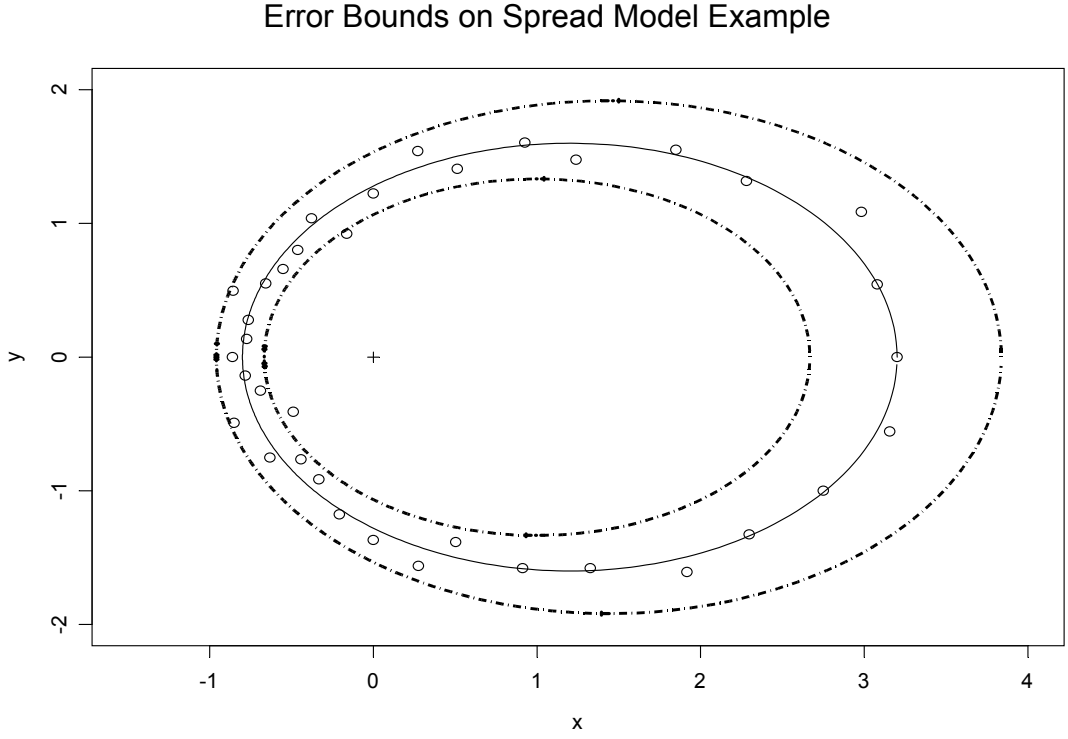

Figure 5. A hypothetical example of fire perimeter data points that contain a lognormal random error component as described by the probability model in (9). The solid line is the simulated fire perimeter corresponding to the null hypothesis that the fire model replicates the mean actual fire. The dashed lines represent 95% confidence limits on the simulated perimeter.

$$P\left\{Z(\frac{\alpha}{2}) < \frac{\ln R(\theta) - \ln r(\theta)}{s} < Z(1-\frac{\alpha}{2})\right\} = 1-\alpha$$

$$P\left\{\ln r(\theta) - Z(1-\frac{\alpha}{2})s < \ln R(\theta) < \ln r(\theta) + Z(1-\frac{\alpha}{2})s\right\} = 1-\alpha \tag{11}$$

where $Z(\cdot)$ is the quantile of the standard normal distribution that corresponds to the cumulative probability of its argument. Under the null hypothesis that the fire model replicates the actual fire, the semi-major axes of the ellipses that correspond to the upper and lower bounds of the approximate 1-α confidence interval for the true perimeter are:

$$\alpha_l = \alpha_m \exp\left(-Z\left(1-\frac{\alpha}{2}\right)s\right)$$

$$\alpha_u = \alpha_m \exp\left(Z\left(1-\frac{\alpha}{2}\right)s\right) \tag{12}$$

Figure 5 shows the simulated perimeter and its 95% confidence limits for our example.

Analysis of the 1996 Bee Fire

I applied the error analysis methodology described above to a fire which we modeled with FARSITE. The Bee Fire occurred in the San Bernardino National Forest, California, USA, over the period 29 June – 3 July 1996. The USDA Forest Service collected data on the environment and growth of the fire for subsequent analysis (Weise and Fujioka, 1998). I focused the analysis on the first two hours of the fire, when the time interval between perimeter observations was shortest.

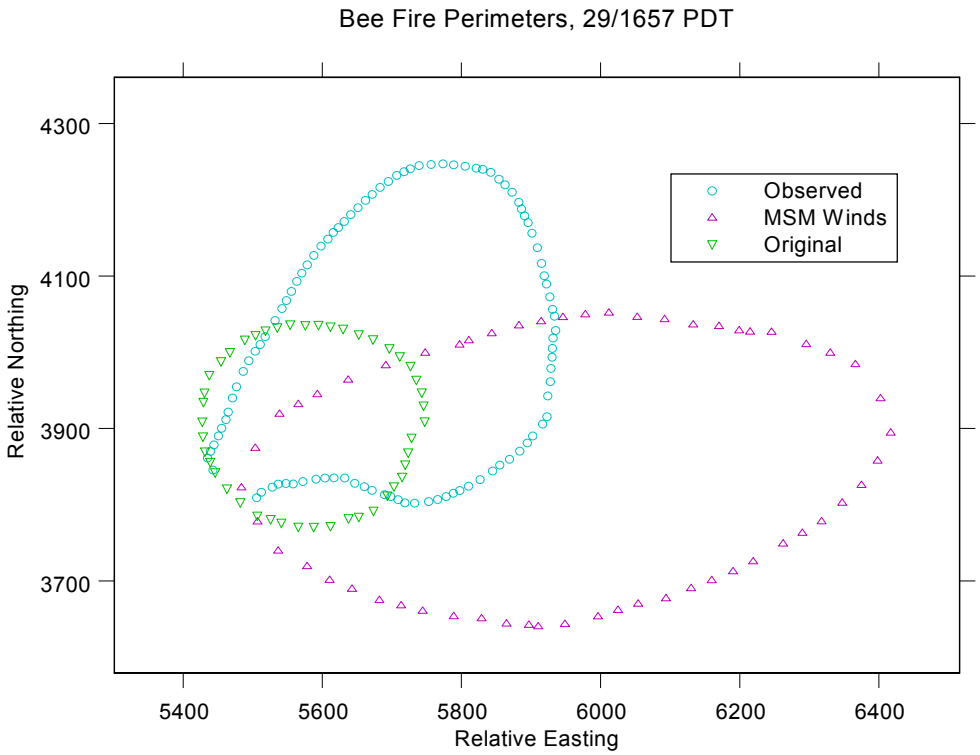

Figure 6. Observed and simulated Bee Fire perimeters on 29 June 1996, 1657 PDT. The perimeter plot marked "MSM Winds" resulted from wind input from a mesoscale weather model, with initial data from 28 June 1996, 1700 PDT. The "Original" perimeter was generated from a nearby wind observation.

The Bee Fire started in the afternoon of 29 June, at the base of the San Jacinto Mountains. The fire began at approximately 680 m above sea level, heading generally northeast. The suppression team contained the fire three days later, but not before the fire covered 3,848 ha. Chaparral was abundant, the predominant fuel type being chamise (*Adenostema fasciculatum* H&A). Over its life, the Bee Fire threatened multiple resources, including the popular mountain community of Idyllwild, to the east.

The temperature at the time of ignition, 1647 Pacific Daylight Time (PDT), was approximately 29° C, relative humidity 19%. Winds blew out of the southwest to northwest at approximately 2 m/s. Less than two hours later, the temperature dropped to 24° C, and relative humidity increased to 24%. Weather simulations with a mesoscale spectral model (Chen et al., 1998) indicated that the sea breeze from the west was approaching the area at about the time of ignition. Figure 7 shows the fire perimeter observed on 29 June 1996 at 1657 PDT, approximately 12 minutes after ignition. Two perimeters simulated by FARSITE are shown for comparison, one based on a wind observation near the fire, and the other based on the winds from the mesoscale spectral model (MSM).

The error analysis for the first perimeter was used to estimate a probability distribution for the spread model errors, which did not resemble a normal distribution. I therefore estimated the error distribution by nonparametric methods, from which I constructed error bounds using the nonparametric density in place of the lognormal density in equation (11) (Figure 7). See Fujioka (2001) for the details of the distributional analysis.

The predicted fire perimeter did not represent the actual fire perimeter well at 1730 PDT. Moreover, the actual fire spread beyond the 95% confidence bound in the northwest direction. The fire appeared to change direction from its initial heading at 1657 PDT.

Summary and conclusions

This paper described a new method to analyze two-dimensional fire spread modeling errors. The method can be used to conduct appropriate statistical tests of hypotheses relevant to the fire spread model, regardless of the choice of fire model. An error correction scheme is proposed, which can be used to adjust model predictions on

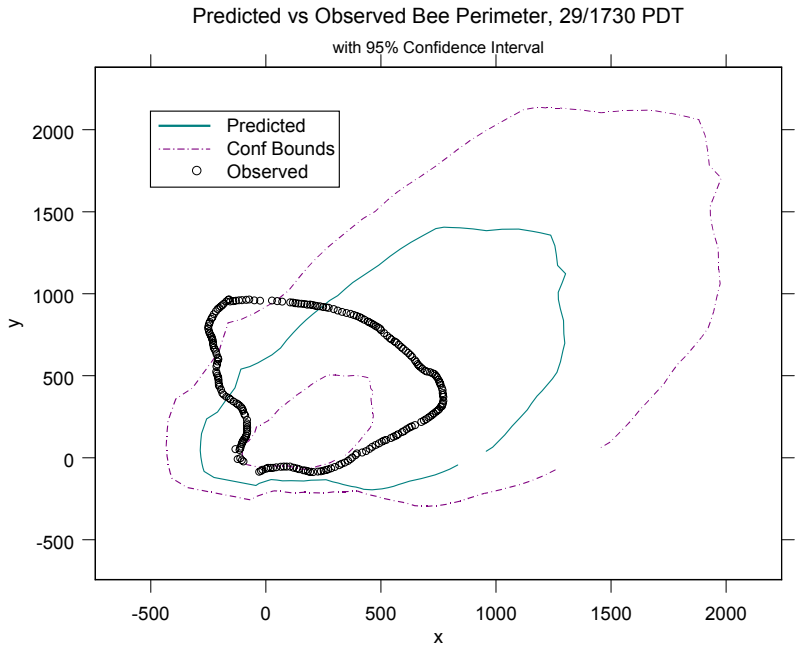

Figure 7. Position and error corrected perimeter prediction for the Bee Fire, 29 June 1996, 1730 PDT, and approximate 95% confidence interval for the true perimeter.

the fly, when the spread model error characteristics are consistent over time. The method also provides for construction of error bounds on predicted perimeters. Application of the error analysis to a southern California case study revealed how complex fire prediction can be. A significant error occurred in the FARSITE simulation of the 1996 Bee Fire, which might have been due to changing wind conditions, or a combination of wind and slope effects that the fire model did not capture. The error analysis also misled the placement of error bounds, because the spread model error was not consistent over time. Further work is necessary on a spatial/temporal error analysis methodology. This should include spatial and temporal dependencies of model errors.

References

Albini, F.A. 1976. Estimating wildfire behavior and effects. USDA Forest Service General Technical Report INT-30. 92 p.

Finney, M.A. 1998. FARSITE: fire area simulator—model development and evaluation. USDA Forest Service Research Paper RMRS-RP-4. 47 p.

Fujioka, F.M. 2001. Characterization and analysis of fire spread modeling errors in an integrated weather/wildland fire model. PhD dissertation (in preparation).

Forestry Canada Fire Danger Group 1992. Development and structure of the Canadian Forest Fire Behavior Prediction System. Forestry Canada Information Rep. ST-X-3, Ottawa, Canada. 63 p.

Chen, S.-C.; Roads, J.O.; Juang, H.-M.H. 1998. Mesoscale fire weather studies. Proceedings, Second Conference on Fire and Forest Meteorology, Phoenix, Arizona. American Meteorological Society, Boston, MA. 134-135.

McArthur, A.G. 1967: Fire behaviour in eucalypt forests. Department of National Development, Forestry and Timber Bureau Leaflet No 107, Canberra, Australia. 36 p.

Noble, I.R., Barry, G.A.V., and Gill, A.M. 1980: MacArthur's fire-danger meters expressed as equations. Australian Journal of Ecology **5**:201-203.

Richards, G.D. 1995: A general mathematical framework for modelling two-dimensional wildland fire spread. International Journal of Wildland Fire **5**:63-72.

Rothermel, R.C. 1972. A mathematical model for predicting fire spread in wildland fuels. USDA Forest Service Research Paper INT-115. 40 p.

Weise, D.R.; Fujioka, F.M. 1998: Comparison of fire spread estimates using weather station observations versus nested spectral model gridded weather. Proceedings, Second Conference on Fire and Forest Meteorology, Phoenix, Arizona. American Meteorological Society, Boston, MA. 75-79.